Research Square

Preprints are preliminary reports that have not undergone peer review.
They should not be considered conclusive, used to inform clinical practice,
or referenced by the media as validated information.

Transient-Based HRV Analysis Reveals Changes in Cardiac Autonomic Dynamics during Repeated Cognitive Engagement

Rémi CHAGNEAUD

remi.chagneaud@u-bordeaux.fr

Univ. Bordeaux, CNRS, Laboratoire IMS, UMR 5218

Laurent M ARSAC

Univ. Bordeaux, CNRS, Laboratoire IMS, UMR 5218

Clément BOUGARD

STELLANTIS AUTO S.A.S

Emmanuelle DIAZ

STELLANTIS AUTO S.A.S

Véronique DESCHODT-ARSAC

Univ. Bordeaux, CNRS, Laboratoire IMS, UMR 5218

Article

Keywords:

Posted Date: November 24th, 2026

DOI: https://doi.org/10.21203/rs.3.rs-11551211/v1

License: This work is licensed under a Creative Commons Attribution 4.0 International License.
Read Full License

Additional Declarations: No competing interests reported.

Abstract

Transitions from rest to cognitive engagement are common in daily life, particularly among human operators. Repeated cognitive demands may induce adaptation or mental fatigue. Heart rate variability (HRV), a marker of cardiac autonomic regulation, may help characterize these responses. We hypothesized that transient HRV dynamics during rest-to-task transitions would reveal physiological adjustments not captured by conventional steady-state measures.

HRV was recorded in 29 healthy young adults during two successive rest-to-task transitions involving visual search and go/no-go tasks. Perceived fatigue, stress, and anxiety were assessed. Conventional HRV indices and entropy were calculated during resting and cognitive phases, while transient low-frequency (LF) and high-frequency (HF) dynamics were characterized during the first minute following each transition using wavelet packet transform analysis.

Response times improved during the second cognitive task despite increased perceived fatigue, accompanied by greater cardiac vagal modulation and preserved HRV entropy. Transient HF and LF dynamics differed significantly between transitions. Moreover, transient slope-based indices showed higher discriminative performance (AUC = 0.65–0.70) than conventional steady-state reactivity indices (AUC = 0.47–0.59).

These findings suggest that transient HRV analysis provides complementary information on cardiac autonomic responses to repeated cognitive engagement, with potential applications for monitoring human operators.

Introduction

Cognitive demand varies continuously in daily life as individuals alternate between rest and tasks imposing different levels of cognitive demand. These fluctuations are particularly relevant in operational environments, including transportation, aviation, and human–machine interaction, where changes in cognitive state may affect both performance and safety [1–3]. Moreover, repeated cognitive demands may produce responses of different nature over time. A better performance can arise thanks to familiarization/habituation or learning phenomenon and illustrates a positive adaptation to repetitions [4]. Alternatively, the need for sustained cognitive engagement may progressively induce mental fatigue and ultimately impair performance [5]. The distinction of these processes requires that the retained physiological markers not only identify different cognitive states but also report on subtle responses when cognitive demand fluctuates across repeated tasks.

Gold-standard brain imaging and neurophysiological techniques such as magnetic resonance imaging (MRI) and electroencephalography (EEG) provide valuable and direct information on changes in cerebral activity [6,7], but their instrumentation and experimental constraints may limit their use for monitoring naturalistic behavior. There is therefore a need for practical physiological methods capable of

characterizing responses to changes in cognitive demand and potentially identifying normal or degraded functional states in human operators non-invasively.

Heart rate variability (HRV) is widely used as a reliable, non-invasive, and readily marker of cardiac autonomic activity, providing valuable insights into the physiological processes associated with cognitive functioning. Conceptual models such as the "Central Autonomic Network" [8,9] or the "Neurovisceral Integration Model" [10–13] emphasize the role of interconnected cortical and subcortical structures in coordinating autonomic, cognitive, and emotional regulation. Within these frameworks, prefrontal cortical regions contribute to the regulation of subcortical and autonomic processes, partly through inhibitory pathways associated with cardiac vagal modulation [14–16]. More recently, neuroimaging studies have further explored the central networks associated with sympathetic and parasympathetic cardiovascular regulation [17]. These findings highlight the importance of considering multiple components of autonomic regulation when investigating brain–heart interactions, rather than focusing exclusively on vagal modulation. Accordingly, examining both low-frequency (LF) and high-frequency (HF) components of HRV may provide complementary information on cardiac autonomic responses to cognitive demands. Beyond conventional HRV indices, growing evidence suggests that the complex organization of neurophysiological regulatory networks is reflected in the nonlinear temporal properties of their physiological outputs. Accordingly, nonlinear HRV analyses [18–21], particularly entropy-based approaches, have emerged as complementary tools for characterizing the complexity of cardiac regulation and its modulation during cognitive activity [22–25].

Studies assessing individual responses to different levels of cognitive demand have typically relied on a standard experimental design wherein HRV markers derived from steady resting periods are compared with those derived from a chosen cognitive task at a given level of difficulty. Such an approach is formalized in the Vagal Tank Theory [26], where vagal activity is indexed by steady-state values across rest, reactivity, and recovery periods. Yet, going one step further, enriched information could be gained from transient, time-resolved dynamics that result from shifts in cognitive demand. In such an approach, autonomic reactivity would be reflected in temporal trajectories, which needs the implementation of transient components analysis to complement steady state indexation of individual behaviors [27]. Among possible approaches, wavelet-based HRV decomposition [28,29], provides a fine time-frequency resolution even when applied to non-stationary signals, which has been useful to characterize specific physiological and cognitive states [30–32]. Recently in this vein, Villatte et al. [33] compared several time-frequency methods and emphasized wavelet-based and empirical decomposition approaches to characterize transient changes in low-frequency (LF) and high-frequency (HF) components of HRV, claiming that transient-derived markers provide information that are not fully captured by conventional spectral analysis. Tracking HRV markers over time can reveal stressor-specific response patterns in relation with individual psychological characteristics, which remain undetected with condition-averaged analyses [34]. However, to the best of our knowledge, little attention has been paid to how the temporal dynamics of LF and HF components unfold during the transition from rest to a cognitive demand and whether these dynamics differ when a cognitive demand with similar demand is repeated.

In the present study, we focused on the novel information potentially gained from transient dynamics of HRV when switching from rest to cognitive demand. For that, a cognitive task based on visual search and go/no-go paradigm, preceded by resting periods, was repeated twice by young healthy participants. Individual autonomic responses were indirectly evaluated by the analysis of HRV through conventional (steady-state) and novel (transient) approaches. Specifically, we compared conventional phase-averaged HRV indices with LF and HF slopes measured during the first minute after each rest-to-task transition. We expected the time-resolved indices to provide complementary information on autonomic adjustments across repeated cognitive engagement

Materials and methods

Participants. Twenty-nine active healthy participants (21 males, 19.6 ± 2 years) from the Faculty of Sports Sciences took part in the study, for which they received credits as part of their academic curriculum. All participants self-reported having no neurological and cardiovascular disorders, vision impairments, or psychological disorders, and none reported the use of different forms of medication. The consumption of alcohol and caffeine, as well as engagement in intense physical activity, was prohibited within the 12 hours preceding the experiment. Informed consent was obtained from all participants for study participation and data publication, in accordance with the Declaration of Helsinki and its amendments. All procedures were approved by the CERSTAPS Ethics Committee.

Experimental Protocol. Upon arrival, participants received standardized instructions and were fitted with a device for continuous cardiac activity monitoring (Polar H10). Then, they completed self-report questionnaires assessing perceived stress, fatigue, and anxiety levels.

The experimental session consisted of four consecutive ten-minute phases. First, participants viewed a neutral wildlife documentary [35] to establish a resting baseline condition (REST1). This phase was immediately followed by a first cognitive task phase (COG1). Participants then completed a second resting phase involving the viewing of a similar neutral documentary (REST2) before performing a second cognitive task phase (COG2).

Transitions between experimental phases were indicated by brief informative sentences, designed to signal the upcoming condition. The experiment was presented on a 27-inch computer monitor, positioned approximately 60 cm from the participant.

Cognitive Task. A dual-task paradigm was implemented using MATLAB (MATLAB 2023b, MathWorks, Natick, MA, USA) and the PsychToolbox toolkit [36]. All stimuli were presented at the center of a black screen. Prior to the experimental session, participants received standardized instructions and completed a practice block to ensure proper understanding of the task and the response keys.

Main task: Visual Search Task (VST)

The main task was grounded on a visual search paradigm [37] designed to elicit the voluntary attentional deployment, interference's inhibition, and sustained attentional control [38], which are core cognitive mechanisms underlying performance in the operational environments [39–41]. Participants had to identify the presence of a target stimulus consisting of an upright red T embedded within a matrix composed of upright blue "T" distractors and inverted red "T" distractors. The matrix contained 5, 10, 15, or 20 elements. In each condition, 50% of the trials included a target stimulus. Each trial began with the presentation of a fixation point for 1000 ms, followed by the stimuli matrix, which remained visible for a maximum duration of 4000 ms. Participants pressed the "T" key as quickly as possible whenever a target stimulus was detected. The next trial began immediately after the response.

Secondary task: Go / No-Go Task (GNGT)

The VST was combined with a go/no-go task to engage dual-task processing capacities. The GNGT occurred only during trials in which the target stimulus was absent. After a delay of 2000 ms, the visual search task disappeared and was replaced by a colored ellipse. Participants were instructed to press the spacebar as quickly as possible when the ellipse was green (Go trials; 70% of trials). When the ellipse was red (No-Go trials; 30% of trials), participants were required to withhold their response. The stimulus remained visible for a maximum duration of 2000 ms. Go and no-go trials occurred in a non-predictable order.

Each cognitive block consisted of 160 trials, presented in a randomized order. Depending on individual response times, total block duration ranged from 9 to 10 min while ensuring balanced experimental conditions (20 trials per matrix size and target condition).

For each task, mean correct response time and error rates (bad inhibition or missed target) were extracted as performance metrics.

Data Collection

Psychological questionnaires. Participants filled out a series of questionnaires assessing perceived stress, perceived fatigue, and anxiety state levels. State anxiety was assessed using the State form of the Spielberger State–Trait Anxiety Inventory (STAI-Y1 [42]), which consists of 20 items evaluating subjective feelings of apprehension, tension, and nervousness. Perceived fatigue and stress were assessed using two visual analog scales (VAS) ranging from 1 to 10, evaluating fatigue ("no fatigue" to "worst imaginable fatigue") and stress ("no stress" to "extremely stressed"), respectively.

Heart Rate Variability. Cardiac interbeat intervals (R-to-R peak interval durations) were continuously recorded using a Polar H10 (Polar, Finland) chest belt connected via Bluetooth to a smartphone application. The RR-interval time series were exported to MATLAB (MATLAB 2023b, MathWorks, Natick, MA, USA) for artifacts inspection and correction using a custom algorithm. Artifacts were identified

when the difference between two successive RR intervals exceeded 250 ms, a threshold considered outside the expected physiological range and potentially indicative of physiological or signal acquisition issues [43,44]. They were replaced by the average of adjacent values. Less than 2% of the total samples in the analyzed dataset were corrupted.

HRV markers derived during steady-states

RR-interval time series were analyzed across the four phases (REST1, COG1, REST2, COG2), during the central 8 minutes of each phase to ensure sufficient signal stability. The mean successive peak-to-peak interval duration (RRmean) and the root-mean-square of the differences between these intervals (RMSSD) were computed. In the time-frequency domain, a wavelet packet transform (WPT) [28] was applied to the 1 Hz resampling RR interval series, which provides fine time-frequency resolution and is particularly suited for non-stationary signals such as HRV. A Hilbert transform was then applied to the third level of WPT to extract the instantaneous amplitude along the signal. The amplitudes were summed over the 0.0625–0.1875 Hz and 0.1875–0.4375 Hz bands to obtain LF and HF, respectively, and squared to compute the corresponding power values. Power values were averaged within each phase to estimate LF, HF, and total power (TP = LF + HF), as well as normalized HF (HFnu), providing information regarding autonomic cardiac modulations. In the nonlinear domain, the complexity of the neurovisceral control of the heart was assessed by computing multi-scale entropy in RR interval time series using the refined composite multiscale entropy (RCMSE) [45]. This method estimates signal complexity across multiple temporal scales and is particularly suitable for short physiological time series (see Eq. 1) [46]. To determine whether the RCMSE values observed in the original RR time series significantly differed from white noise, the same procedure was applied to a surrogate series, generated by randomly shuffling the original data to emulate the properties of white noise, that is to say, decreased values of entropy over scale. RCMSE was calculated as follows:

$$RCMSE(x,\ \tau\ ,\ m, r)\ =\ -\ln\left(\frac{\sum_{k=1}^{\tau} n_{k,\ \tau}^{m+1}}{\sum_{k=1}^{\tau} n_{k,\ \tau}^{m}}\right), \text{ Eq. (1)}$$

where *x* is the RR time series, τ the scale factor, *m* the sequence length considered (here, m = 2), and *r* is the tolerance factor (here, 0.15). The RCMSE value was calculated for each scale, τ, from τ = 1 to τ = 3. Finally, the cardiac entropy index (Ei) was obtained by calculating the area under the curve of RCMSE values, using the trapezoidal rule. Following the recommendations of Gow et al. [47], entropy measures were computed after preprocessing the time series using Empirical Mode Decomposition (EMD) [48]. This technique decomposes the signal into intrinsic mode functions (IMFs) and a residual component. To mitigate low-frequency drift, recognized as a source of bias in entropy estimation [47], the residual component and the last IMF were removed prior to analysis.

HRV markers derived during transition phases

In addition to the steady-state-based analysis, a transient-based approach was used to characterize the temporal dynamics of HRV during shifts from resting periods to cognitive tasks. The RR time series were analyzed during the minute after the shifts between the resting phases (REST1 and REST2) and the tasking phases (COG1 and COG2). These shifts are defined as the transition phases (first transition, RC1 and second transition, RC2). During each transition, the HF and LF components power values calculated from a wavelet packet transform (WPT) as described before were averaged over 30-s windows with a 20-s overlap, yielding a 10-s resolution with enough data points per window [28,49]. Temporal dynamics of the LF power and HF power were quantified using a slope analysis applied to the 5 post-transition windows (Fig. 2). These acute responses were modeled using two linear regressions over windows 1–3 (S1, very short response) and 3–5 (S2, short response).

Statistical analysis. Values are expressed as means ± standard deviations (SD). To improve normality, reduce skewness and stabilize variance, cardiac autonomic markers were natural log-transformed prior to statistical analyses. The assumption of normality was then assessed using the Shapiro–Wilk test. All statistical tests were performed with an alpha level (α) of 0.05.

Comparison analysis

The PRE-POST comparisons of psychological indices were performed using paired-sample t-tests for normally distributed data with Cohen's d reported as effect size, or alternatively by using the Wilcoxon signed-rank tests in case of non-normally distributed data, with rank-biserial correlation (r_{rb}) reported as effect size.

Comparisons between the different phases (REST1, COG1, REST2, COG2) of the mean autonomic cardiac markers (RMSSD, HF, LF, TP, HFnu, Entropy) calculated using the average-based approach were performed using one-way repeated-measures analysis of variance (ANOVA). In cases of significant main effects, post-hoc comparisons with Holm-Bonferroni correction were conducted. Comparisons between transitions (RC1, RC2) of the indices derived from the transient-based approach (HF component and LF component dynamics) were performed using two-way repeated-measures analysis of variance (ANOVA 2RM). For all repeated-measures ANOVAs, sphericity was assessed using Mauchly's test. When the assumption of sphericity was not met, Greenhouse-Geisser corrections were applied.

Sensitivity analysis

Receiver Operating Characteristic (ROC) curve analyses were performed to compare the discriminative performance of mean cardiac markers and transient markers between the two transitions, RC1 and RC2. Classification performance will be assessed using the area under the ROC curve (AUC) and the Youden J index. Mean cardiac markers will be expressed as the relative changes from the resting state, yielding reactivity indices comparable to the transient markers.

Statistical analyses were conducted using JASP (version 0.95.4, JASP Team, 2025) and RStudio (version 4.5.2; R Core Team, 2025). and figures were generated using MATLAB functions.

Results

Cognitive performance. Mean correct response times, as the primary measure of cognitive performance, were significantly shorter during COG2 than during COG1 for both the visual search task (920 ± 10 ms vs. 1039 ± 105 ms; *t(28) = -11.017, p < 0.001, d = -2.046*) and the go/no-go task (493 ± 79 ms vs. 529 ± 74 ms; *t(28) = -3.945, p < 0.001, d = -0.733*). Error counts did not differ significantly between COG2 and COG1, either for the visual search task (0.7 ± 0.8 vs. 1.2 ± 1.3) or for the go/no-go task (2.5 ± 1.5 vs. 2.1 ± 1.1). These results indicate better cognitive performance during the second repetition of the task.

Anxiety, stress, and fatigue. From PRE to POST experiment, state anxiety scores did not change significantly (30.8 ± 7.1 to 29.8 ± 6.8; *t(28) = 1.052, p = 0.302, d = 0.195*), whereas fatigue increased (3.6 ± 1.6 to 4.6 ± 1.9; *z = − 2.776, p = 0.005, rrb = − 0.676*) and perceived stress decreased (2.5 ± 1.2 to 2.0 ± 0.6; *z = 2.551, p = 0.010, rrb = 0.802*). Overall, the experimental protocol induced fatigue without increasing anxiety or stress.

Cardiac autonomic markers.

Steady-states-based approach: HRV markers derived during experimental phases

Table 1
Cardiac autonomic markers calculated from RR-interval time series in time, time-frequency and non-linear domains during REST1, COG1, REST2, and COG2. Values are reported as mean ± standard deviation. Mean RR = mean interbeat interval duration; LnRMSSD = log-transformed root-mean-square of successive differences; LnLF = log-transformed low-frequency power in HRV; LnHF = log-transformed high-frequency power in HRV; LnTP = log-transformed total-frequency power in HRV; HFnu = index of sympatho-vagal balance; Ei: entropy index. Significant differences are expressed as follows: difference with REST1: *; difference with COG1: $^{\#}$; difference with REST2: °. Levels of significance are explained in the text.

Physiological markers	REST1	COG1	REST2	COG2
Mean RR (ms)	866 ± 128	854 ± 123	884 ± 125 °	879 ± 116 * #
LnRMSSD (ms)	3.71 ± 0.41	3.81 ± 0.41 *	3.77 ± 0.39	3.91 ± 0.40 * ° #
LnLF (ms²)	7.84 ± 0.61	7.63 ± 0.61	7.88 ± 0.61	7.82 ± 0.62
LnHF (ms²)	6.79 ± 0.85	7.05 ± 0.79 * °	6.84 ± 0.87	7.19 ± 0.78 * ° #
LnTP (ms^2)	8.18 ± 0.60	8.12 ± 0.61	8.22 ± 0.62	8.30 ± 0.58
HFnu (a.u.)	0.28 ± 0.13	0.37 ± 0.13 * °	0.28 ± 0.12	0.36 ± 0.15 * °
Ei (a.u.)	3.72 ± 0.48	4.14 ± 0.36 * °	3.52 ± 0.50 *	4.09 ± 0.27 * °

The cognitive task phases induced an increase in cardiac vagal markers: LnRMSSD ($F(2.17, 60.76) = 10.92$, $p < 0.001$, $\eta^2 = 0.28$), LnHF ($F(2.03, 59.82) = 12.44$, $p < 0.001$, $\eta^2 = 0.31$) and HFnu ($F(3, 84) = 14.80$, $p < 0.001$, $\eta^2 = 0.35$) differed significantly across phases, with higher values during COG1 and COG2 than during rest phases. This response was more pronounced during COG2, as LnRMSSD and LnHF were also significantly higher during COG2 than during COG1 ($t(28) = 4.85$, $p = < 0.001$, $d = 0.26$ and $t(28) = 3.43$, $p = 0.007$, $d = 0.17$, respectively).

Neither LnLF ($F(2.24, 62.70) = 2.75$, $p = 0.066$, $\eta^2 = 0.09$) nor LnTP ($F(2.15, 60.35) = 2.04$, $p = 0.136$, $\eta^2 = 0.07$) differed significantly across experimental phases.

The entropy index (Ei) also differed significantly across experimental conditions ($F(1.88, 52.60) = 32.14$, $p < 0.001$, $\eta^2 = 0.53$). Ei values were higher during cognitive periods, with COG1 being higher than BAS1 ($t(28) = 6.29$, $p < 0.001$, $d = 1.01$) and BAS2 ($t(28) = 7.81$, $p < 0.001$, $d = 1.50$), and COG2 being also higher than BAS1 ($t(28) = 4.20$, $p < 0.001$, $d = 0.89$) and BAS2 ($t(28) = 5.98$, $p < 0.001$, $d = 1.38$). It may also be noted that a significant drop in entropy was observed between REST1 and REST2 ($t(28) = -3.98$, $p < 0.001$, $d = -0.49$).

Transient-based approach: HRV markers derived during transition phases

Table 2

Cardiac autonomic dynamics indices derived from the time-resolved analysis of the HF and LF components of heart rate variability during the first (RC1) and second (RC2) transitions from rest (REST1 and REST2) to cognitive task (COG1 and COG2). Values are reported as mean ± standard deviation. S1 = slope of the very-short-term response; S2 = slope of the short-term response. Two-way repeated-measures ANOVAs (Transitions × Slopes) were performed separately for the HF and LF components. Significant main effects are indicated as follows: main effect of transition (RC1 vs RC2): *** $p < 0.001$, ** $p < 0.01$, * $p < 0.05$; main effect of slope (S1 vs S2): # $^{\#\#\#}$ $p < 0.001$, $^{\#\#}$ $p < 0.01$, $^{\#}$ $p < 0.05$.

HF component	**RC1**	**RC2 *****
S1	− 0.043 ± 0.212	0.123 ± 0.332
S2	− 0.058 ± 0.361	0.170 ± 0.302
LF component	**RC1**	**RC2 *****
S1	0.114 ± 0.447	0.173 ± 0.390
S2 $^{\#\#\#}$	− 0.464 ± 0.539	− 0.122 ± 0.362

Regarding the HF component, the time course of HF following the rest-to-task transition differed between RC2 and RC1 ($F(1, 28) = 19.90$, $p < 0.001$, $\eta^2 = 0.16$). The slopes reflecting very-short-term responses (HF-S1) and short-term responses (HF-S2) were both negative during RC1 but both positive during RC2. HF-S1 and HF-S2 did not differ from each other ($F(1, 28) = 0.12$, $p = 0.727$, $\eta^2 = 0.01$), and this pattern did not depend on transition, as shown by the absence of a slopes x transitions interaction ($F(1, 28) = 0.35$, $p = 0.560$, $\eta^2 = 0.01$). This suggests a consistent direction of response during the early seconds after the transition.

Regarding the LF component, the time course of LF following the rest-to-task transition differed between RC1 and RC2 ($F(1, 28) = 8.15$, $p = 0.008$, $\eta^2 = 0.06$). In both conditions, the slope reflecting very-short-term responses (LF-S1) was positive, whereas the slope reflecting short-term responses (LF-S2) was negative; this difference between LF-S1 and LF-S2 was significant ($F(1, 28) = 32.71$, $p < 0.001$, $\eta^2 = 0.27$). The difference between conditions was most apparent for LF-S2, which showed the steepest negative slope of all in RC1, although the slopes x transitions interaction did not reach significance ($F(1, 28) = 3.67$, $p = 0.06$, $\eta^2 = 0.03$).

Sensitivity analysis

Roc analysis was performed to assess the ability of either transient- or steady-state-based HRV markers to discriminate responses during the first (RC1) and the second transition (RC2). The highest AUC values were obtained for LF-S2 (AUC = 0.70), HF-S2 (AUC = 0.67), and HF-S1 (AUC = 0.65). These markers also exhibited the highest Youden's *J* indices, indicating the best balance between sensitivity and specificity.

Table 3

Discriminative performance of HRV markers for distinguishing the first from the second rest-to-task transition (RC1 vs. RC2). For each marker, the area under the ROC curve (AUC) and Youden's index (J = sensitivity + specificity − 1) are reported. Markers are ranked by decreasing AUC. LF-S1, LF-S2, HF-S1 and HF-S2: slopes of the transient LF and HF components extracted by wavelet packet transform; Δ: difference between task and rest steady-state values (HF, Ei, HFnu);

Markers	***AUC***	***J***
LF-S2	0.70	0.38
HF-S2	0.67	0.34
HF-S1	0.65	0.31
Δ HF	0.59	0.24
Δ Ei	0.56	0.24
LF-S1	0.52	0.17
Δ HFnu	0.47	0.07

Discussion

The present study focused on autonomic responses during repeated shifts in cognitive demand. Transient markers were derived from the time course of HF and LF components of HRV, obtained using wavelet packet decomposition (WPT) and Hilbert transform. This approach allowed capturing early autonomic dynamics that follow each two experimental rest-to-task transitions to gain improved information on individual behaviors. The main finding was that, despite the repetition of the same task in COG1 and COG2, the successive rest-to-task transitions (RC1 and RC2) elicited distinct autonomic responses. This was reflected in HRV metrics, with transient markers offering a finer view on early autonomic dynamics. A novel and original finding here was that transient-based HRV markers showed the highest sensitivity to differentiate the two successive rest-to-task transitions, outperforming markers extracted from steady-state autonomic status during each task. These observations suggest using time-resolved analysis of HRV applied to transitory periods when human operators switch between cognitive demand in a number of contexts.

Steady-state HRV responses to cognitive tasks

Every autonomic marker derived from steady states, RMSSD, HF power, and normalized HF power (HFnu), pointed to an increased vagal activity during each phase of cognitive engagement, COG1 and COG2. These findings are not new, and they are in line with the conceptual framework of neurovisceral integration [11,13] that emphasizes a functional relationship between prefrontal regulatory networks, cognitive functioning and cardiac vagal activity [13,15,16]. Vagally mediated responses generally vary according to task characteristics and the resulting need of attentional resources, and behavioral regulations. In our conditions, a rise rather than a decrease in vagally mediated HRV during COG1 and COG2 may reflect the recruitment of regulatory processes that supports task performance. In line of the analyses of steady state HRV responses, one of interesting results relies on the higher multiscale entropy marker during both cognitive phases than during resting periods. This observation is consistent with previous findings suggesting the adding value of this marker to the understanding of complex neural organization and brain-heart interactions challenged by cognitive tasks [22–25].

Cardiac vagal modulation during repeated cognitive engagement

Beyond the overall increase in cardiac vagal modulation observed during cognitive engagement, the comparison between COG1 and COG2 revealed additional physiological adjustments, primarily characterized by higher vagally mediated HRV indices during COG2. Although participants performed identical tasks in both conditions, performance improved during COG2, as reflected by shorter response times in both the visual search and go/no-go paradigms, without significant changes in error rates. Concurrently, participants reported increased fatigue and decreased stress over the experimental session, while anxiety remained unchanged. Together, these findings suggest that task familiarization, habituation, or more effective task-related self-regulation may have contributed to improved performance despite increased perceived fatigue. This pattern is consistent with the Neurovisceral Integration Model proposed by Thayer and Lane [13,15,16], which emphasizes the relationship between cardiac vagal regulation and neural networks involved in cognitive and emotional self-regulation. It can also be interpreted within the framework of the Vagal Tank Theory [26], which highlights the relevance of cardiac vagal activity and reactivity in adaptive responses to cognitive demands. In the present study, the association between improved task performance and enhanced cardiac vagal modulation during COG2 may therefore reflect a more favorable regulatory response to repeated cognitive engagement.

Transient HRV dynamics reveal additional adjustments

The main methodological contribution of the present study emerged from the analysis of transient HRV dynamics during the two rest-to-task transitions. Whereas steady-state comparisons between COG1 and COG2 primarily revealed differences in vagally mediated indices, time-resolved analyses identified significant effects of rest-to-task transition encompassing both HF and LF dynamics. The fact that both HF and LF transient components carry information on individual responses indicates that early

autonomic regulations after switching from rest to task provides information that is not fully captured by indices derived from the steady-state approach of COG1 and COG2. Regarding HF, temporal slopes were negative during the first transition (RC1) but positive during the second transition (RC2), revealing contrasting patterns of early HF modulation during repeated cognitive engagement. These findings extend the steady-state observations by showing that differences in vagally mediated HRV between COG1 and COG2 were also reflected in the initial dynamics following task onset. More importantly, transient LF dynamics also differed between RC1 and RC2. Both transitions were characterized by an initial positive LF slope followed by a negative slope, that may suggest that the temporal evolution of LF power is sensitive to cognitive engagement, even though the mean values calculated during the steady state fail to distinguish rest from cognitive tasks.

ROC analysis provided further support for the potential relevance of transient HRV indices. Among all indices examined, the late LF slope (LF-S2) yielded the highest observed discriminative performance between RC1 and RC2 (AUC = 0.70), followed by the HF-derived indices HF-S2 (AUC = 0.67) and HF-S1 (AUC = 0.65). These values exceeded those obtained with conventional steady-state reactivity indices (AUC = 0.47–0.59). These results suggest that transient LF and HF dynamics may capture aspects of cardiac autonomic responses to repeated cognitive engagement that are not fully represented by conventional condition-averaged HRV measures.

The transient-based analysis in our conditions introduced the idea that the sympathetic regulation, which is thought to contribute substantially to the LF component, may play a meaningful role when it comes to evaluate individual profiles during repeated task repetition. In this respect, recent neuroimaging findings have highlighted the involvement of distinct but interacting central autonomic networks in sympathetic and parasympathetic cardiovascular regulation [17] supporting a broader conceptual approach to brain–heart interactions that extends beyond vagal modulation alone. The present results are consistent with the value of this broader perspective: while steady-state differences between repeated cognitive tasks were predominantly reflected in vagally mediated HRV indices, transient analyses also revealed changes in LF dynamics. Consequently, the interest of transient HRV analysis may lie not only in its ability to characterize early adjustments more precisely, but also in its capacity to reveal contributions from frequency components that appear relatively uninformative when averaged over steady-state phases. Examining LF and HF trajectories jointly may therefore offer a more comprehensive description of cardiac autonomic responses to changing cognitive demands.

One limitation must be considered when drawing conclusions from this study. Respiratory activity was not recorded throughout the experimental procedure. Given that respiratory rate can significantly influence HRV oscillations, particularly in the HF band [56], the transient HF and LF profiles cannot be attributed solely to changes in cardiac autonomic regulation. Future studies combining HRV with continuous respiratory measurements will be necessary to determine the respective contributions of autonomic processes to this transition dynamic.

In conclusion, transient HRV analysis complements conventional steady-state approaches by revealing differences in the temporal organization of cardiac autonomic responses during repeated shifts from rest to cognitive engagement. Whereas steady-state comparisons primarily identified changes in vagally mediated indices between repeated cognitive tasks, transient analyses revealed significant differences in both HF and LF dynamics. Notably, the late LF slope showed the highest observed discriminative performance, despite the absence of significant differences in mean LF power between cognitive phases. These findings highlight the value of extending HRV analysis beyond physiological states to the transitions linking them and suggest that joint analysis of transient HF and LF dynamics may provide useful complementary information for investigating cardiac autonomic responses in dynamic operational environments.

Declarations

Author contributions statement

V.D.A conceptualized the research question, designed the study, and wrote the paper. R.C. designed and executed the study, conducted the analyses and wrote the paper. L.M.A. contributed to writing the manuscript. C.B and E.D. contributed to conducting the study and revised the manuscript. All authors reviewed the manuscript.

Ethics statement

The present study was approved by the Ethics Committee, the CERSTAPS (Approval No. IRB00012476-2026-26-04-488) and conformed to the standards set by the Declaration of Helsinki (2024 revised version).

Informed consent

Written informed consent was obtained from all individual participants included in the study.

Additional information

The authors declare no competing interests.

Funding

This research was funded by a CIFRE grant, No. 2026/0049, which was awarded by the Association Nationale de la Recherche et de la Technologie (ANRT) to Stellantis Auto SAS in support of the work of

Rémi CHAGNEAUD, PhD student.

Author Contribution

V.D.A conceptualized the research question, designed the study, and wrote the paper. R.C. designed and executed the study, conducted the analyses and wrote the paper. L.M.A. contributed to writing the manuscript. C.B and E.D. contributed to conducting the study and revised the manuscript. All authors reviewed the manuscript.

Data Availability

The dataset generated and analyzed during the current study is available from the corresponding author upon reasonable request.

References

1. Ma, J., Wu, Y., Rong, J. & Zhao, X. A systematic review on the influence factors, measurement, and effect of driver workload. *Accid. Anal. Prev.* **192**, 107289 (2023).
2. Loft, S., Sanderson, P., Neal, A. & Mooij, M. Modeling and Predicting Mental Workload in En Route Air Traffic Control: Critical Review and Broader Implications. *Hum. Factors J. Hum. Factors Ergon. Soc.* **49**, 376–399 (2007).
3. Zamarreño Suárez, M. et al. Understanding the research on air traffic controller workload and its implications for safety: A science mapping-based analysis. *Saf. Sci.* **176**, 106545 (2024).
4. Haith, A. M. & Krakauer, J. W. The multiple effects of practice: skill, habit and reduced cognitive load. *Curr. Opin. Behav. Sci.* **20**, 196–201 (2018).
5. Habay, J. et al. Mental Fatigue Negatively Impacts Cognitive and Physical Performance Outcomes: A Large-Scale Randomized Crossover Trial. *Med. Sci. Sports Exerc.* **58**, 225–241 (2026).
6. Gonsalves, B. D., Cohen, N. J., Brain & Imaging Cognitive Processes, and Brain Networks. *Perspect. Psychol. Sci. J. Assoc. Psychol. Sci.* **5**, 744–752 (2010).
7. Beppi, C., Ribeiro Violante, I., Scott, G. & Sandrone, S. EEG, MEG and neuromodulatory approaches to explore cognition: Current status and future directions. *Brain Cogn.* **148**, 105677 (2021).
8. Benarroch, E. E. The Central Autonomic Network: Functional Organization, Dysfunction, and Perspective. *Mayo Clin. Proc.* 68, 988–1001 (1993).
9. Benarroch, E. Central Autonomic Control. in *Clinical autonomic disorders: evaluation and management* 9–12 (2012). 10.1016/B978-0-12-386525-0.00002-0
10. Thayer, J. F. & Lane, R. D. A model of neurovisceral integration in emotion regulation and dysregulation. *J. Affect. Disord*. **61**, 201–216 (2000).

11. Thayer, J. F. & Lane, R. D. Claude Bernard and the heart-brain connection: further elaboration of a model of neurovisceral integration. *Neurosci. Biobehav Rev.* **33**, 81–88 (2009).
12. Smith, R., Thayer, J. F., Khalsa, S. S. & Lane, R. D. The hierarchical basis of neurovisceral integration. *Neurosci. Biobehav Rev.* **75**, 274–296 (2017).
13. Thayer, J. F., Hansen, A. L., Saus-Rose, E. & Johnsen, B. H. Heart rate variability, prefrontal neural function, and cognitive performance: the neurovisceral integration perspective on self-regulation, adaptation, and health. *Ann. Behav. Med. Publ Soc. Behav. Med.* **37**, 141–153 (2009).
14. Barber, A. D. et al. Parasympathetic arousal-related cortical activity is associated with attention during cognitive task performance. *NeuroImage* **208**, 116469 (2020).
15. Forte, G., Favieri, F. & Casagrande, M. Heart Rate Variability and Cognitive Function: A Systematic Review. *Front Neurosci* **13**, (2019).
16. Forte, G. & Casagrande, M. The intricate brain–heart connection: The relationship between heart rate variability and cognitive functioning. *Neuroscience* **565**, 369–376 (2025).
17. Valenza, G., Ciò, F. D., Toschi, N. & Barbieri, R. Sympathetic and parasympathetic central autonomic networks. *Imaging Neurosci.* **2**, imag200094 (2024).
18. Goldberger, A. L. Non-linear dynamics for clinicians: chaos theory, fractals, and complexity at the bedside. *Lancet* **347**, 1312–1314 (1996).
19. Goldberger, A. L., Rigney, D. R. & West, B. J. Chaos and fractals in human physiology. *Sci. Am.* **262**, 42–49 (1990).
20. Costa, M., Goldberger, A. L. & Peng, C. K. Multiscale Entropy Analysis of Complex Physiologic Time Series. *Phys. Rev. Lett.* **89**, 068102 (2002).
21. Costa, M., Goldberger, A. L. & Peng, C. K. Multiscale entropy analysis of biological signals. *Phys. Rev. E.* **71**, 021906 (2005).
22. Arsac, L. M. Entropy-Based Multifractal Testing of Heart Rate Variability during Cognitive-Autonomic Interplay. *Entropy* **25**, 1364 (2023).
23. Bouny, P., Arsac, L., Touré, E. & Deschodt-Arsac, V. Entropy and Multifractal-Multiscale Indices of Heart Rate Time Series to Evaluate Intricate Cognitive-Autonomic Interactions. *Entropy* **23**, 663 (2021).
24. Blons, E. et al. Alterations in heart-brain interactions under mild stress during a cognitive task are reflected in entropy of heart rate dynamics. *Sci Rep* **9**, (2019).
25. Blons, E., Arsac, L. & Gilfriche, P. Deschodt-Arsac, V. Multiscale Entropy of Cardiac and Postural Control Reflects a Flexible Adaptation to a Cognitive Task. *Entropy* **21**, 1024 (2019).
26. Laborde, S., Mosley, E. & Mertgen, A. Vagal Tank Theory: The Three Rs of Cardiac Vagal Control Functioning – Resting, Reactivity, and Recovery. *Front. Neurosci.* **12**, 458 (2018).
27. Mainardi, L. T., Bianchi, A. M. & Cerutti, S. Time-frequency and time-varying analysis for assessing the dynamic responses of cardiovascular control. *Crit. Rev. Biomed. Eng.* **30**, 175–217 (2002).

28. Tanaka, K. & Hargens, A. R. Wavelet packet transform for R-R interval variability. *Med. Eng. Phys.* **26**, 313–319 (2004).
29. Pichot, V. et al. Wavelet transform to quantify heart rate variability and to assess its instantaneous changes. *J. Appl. Physiol.* **86**, 1081–1091 (1999).
30. Boffet, A., Arsac, L., Ibanez, V. & Sauvet, F. Deschodt-Arsac, V. Detection of Cognitive Load Modulation by EDA and HRV. *Sensors* **25**, 2343 (2025).
31. Geng, D. Y., Zhao, J., Wang, C. X. & Ning, Q. A decision support system for automatic sleep staging from HRV using wavelet packet decomposition and energy features. *Biomed. Signal. Process. Control*. **56**, 101722 (2020).
32. Akar, S. A., Kara, S. & Bilgiç, V. Investigation of heart rate variability in major depression patients using wavelet packet transform. *Psychiatry Res.* **238**, 326–332 (2016).
33. Villatte, B., Kizuk, S., Lina, J. M., Vinet, A. & Hebert, S. Heart rate variability (HRV) during acute stress: a comparison of three methods for time–frequency analysis. *Physiol Meas* **47**, (2026).
34. Villatte, B. et al. Temporal dynamics of heart rate variability reveal stressor-specific autonomic patterns: a multi-stressor study. *Front Neurosci* **20**, (2026).
35. *Le plus beau pays du monde: Opus 2*. (Boréales; AB Productions, (2015).
36. Kleiner, M. et al. What's new in Psychtoolbox-3. *Perception* 36, 1–16 (2007).
37. Stoet, G. Sex differences in search and gathering skills. *Evol. Hum. Behav.* **32**, 416–422 (2011).
38. Petersen, S. E. & Posner, M. I. The Attention System of the Human Brain: 20 Years After. *Annu. Rev. Neurosci.* **35**, 73–89 (2012).
39. Roca, J., Crundall, D., Moreno-Ríos, S., Castro, C. & Lupiáñez, J. The influence of differences in the functioning of the neurocognitive attentional networks on drivers' performance. *Accid. Anal. Prev.* **50**, 1193–1206 (2013).
40. Yan, L. et al. An Evaluation of Executive Control Function and Its Relationship with Driving Performance. *Sensors* **21**, 1763 (2021).
41. Pergantis, P., Bamicha, V., Chaidi, I. & Drigas, A. Driving Under Cognitive Control: The Impact of Executive Functions in Driving. *World Electr. Veh. J.* **15**, 474 (2024).
42. Spielberger, C., Gorsuch, R., Lushene, R., Vagg, P. & Jacobs, G. *Manual for the State-Trait Anxiety Inventory (Form Y1 – Y2)*. *Palo Alto, CA: Consulting Psychologists Press;* vol. IV (1983).
43. Alcantara, J. M. A. et al. Impact of Using Different Levels of Threshold-Based Artefact Correction on the Quantification of Heart Rate Variability in Three Independent Human Cohorts. *J. Clin. Med.* **9**, 325 (2020).
44. *Cardiac Electrophysiology: From Cell to Bedside*. (Saunders, Philadelphia, (1995).
45. Wu, S. D., Wu, C. W., Lin, S. G., Lee, K. Y. & Peng, C. K. Analysis of complex time series using refined composite multiscale entropy. *Phys. Lett. A*. **378**, 1369–1374 (2014).
46. Humeau-Heurtier, A. The Multiscale Entropy Algorithm and Its Variants: A Review. *Entropy* **17**, 3110–3123 (2015).

47. Gow, B., Peng, C. K., Wayne, P. & Ahn, A. Multiscale Entropy Analysis of Center-of-Pressure Dynamics in Human Postural Control: Methodological Considerations. *Entropy* **17**, 7926–7947 (2015).
48. Huang, N. et al. The empirical mode decomposition and the Hilbert spectrum for nonlinear and non-stationary time series analysis. *Proc. R. Soc. Lond. Ser. Math. Phys. Eng. Sci.* 454, 903–995 (1998).
49. Takahashi, N., Kuriyama, A., Kanazawa, H., Takahashi, Y. & Nakayama, T. Validity of spectral analysis based on heart rate variability from 1-minute or less ECG recordings. *Pacing Clin. Electrophysiol.* **40**, 1004–1009 (2017).
50. Christou-Champi, S., Farrow, T. F. D. & Webb, T. L. Automatic control of negative emotions: Evidence that structured practice increases the efficiency of emotion regulation. *Cogn. Emot.* **29**, 319–331 (2015).
51. Nuamah, J. Effect of recurrent task-induced acute stress on task performance, vagally mediated heart rate variability, and task-evoked pupil response. *Int. J. Psychophysiol.* **198**, 112325 (2024).
52. Grissom, N. & Bhatnagar, S. Habituation to repeated stress: Get used to it. *Neurobiol. Learn. Mem.* **92**, 215–224 (2009).
53. Barber, A. D. et al. Contributions of parasympathetic arousal-related activity to cognitive performance in First Episode Psychosis patients and controls. *Biol. Psychiatry Cogn. Neurosci. Neuroimaging*. **8**, 181–188 (2023).
54. Magnon, V., Dutheil, F. & Vallet, G. T. The heart to make the right choice: Vagal (re)activity and recovery predict advantageous decision-making. *Physiol. Behav.* **254**, 113911 (2022).
55. Forte, G., Morelli, M. & Casagrande, M. Heart Rate Variability and Decision-Making: Autonomic Responses in Making Decisions. *Brain Sci.* **11**, 243 (2021).
56. Shaffer, F. & Ginsberg, J. P. An Overview of Heart Rate Variability Metrics and Norms. *Front. Public. Health*. **5**, 258 (2017).

Figures

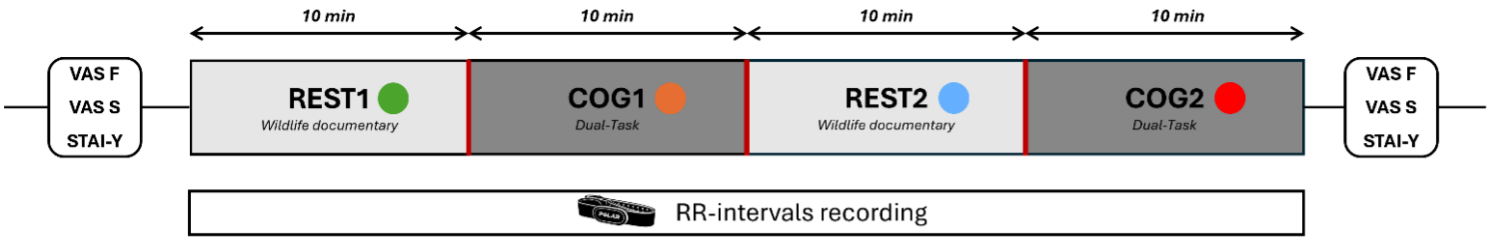

Figure 1

Experimental protocol. VAS F: Visual Analog Scale of perceived Fatigue; VAS S: Visual Analog Scale of perceived Stress; STAI-Y: questionnaire of anxiety state; REST1: neutral video; COG1: dual task; REST2: neutral video; and COG2: dual task.

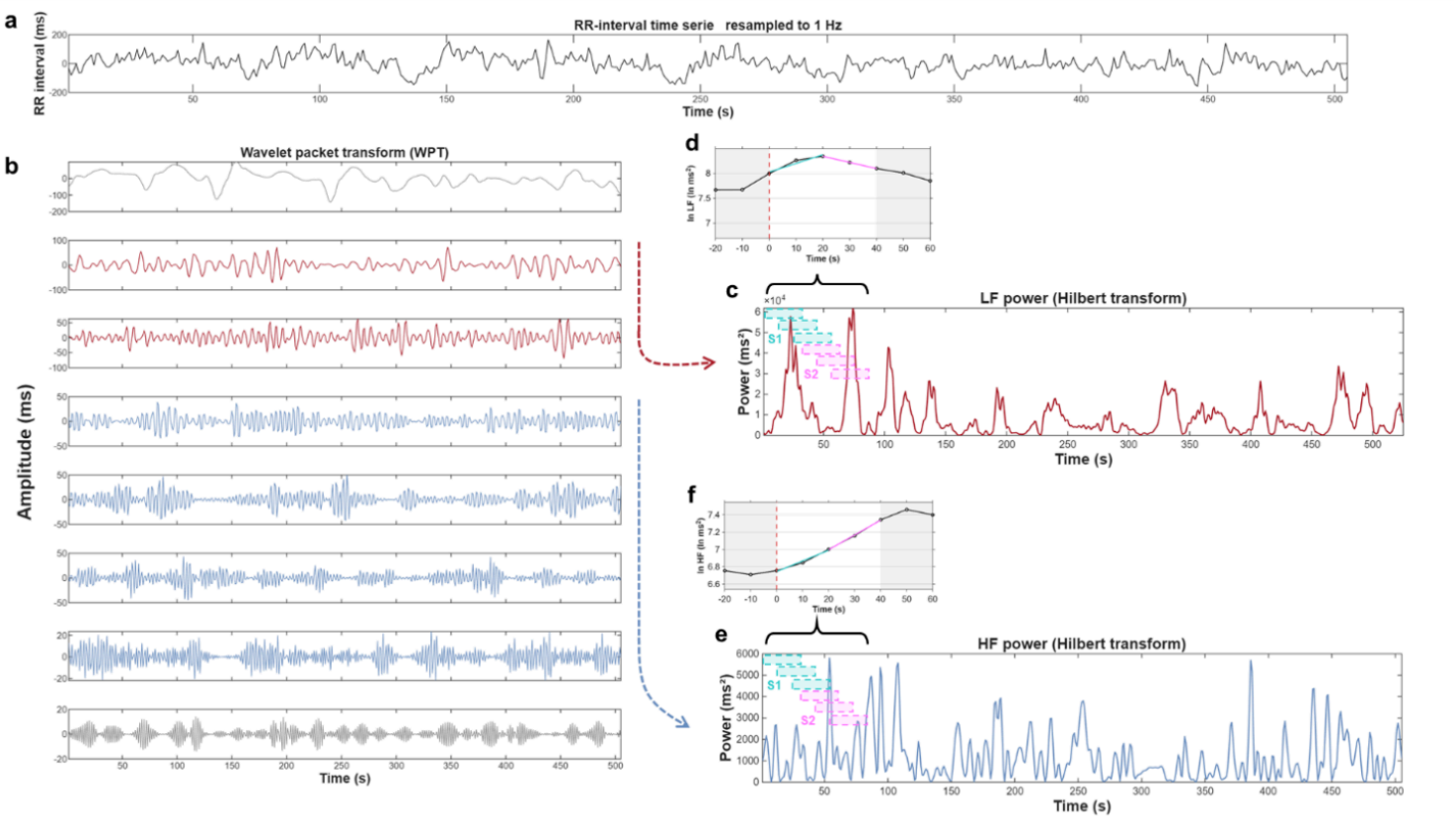

Figure 2

Time-frequency processing pipeline for the extraction of LF and HF dynamics. (a) RR-interval time series resampled at 1 Hz. (b) Level-3 wavelet packet transform (WPT) decomposition of the RR series into eight frequency sub-bands. The nodes used to reconstruct the LF band are shown in red and those used for the HF band in blue; grey nodes were not retained. (c, e) Instantaneous LF (c) and HF (e) power obtained by Hilbert transform of the reconstructed band signals. Dashed boxes show the successive 30-s analysis windows, with a 20s overlap, used to compute S1 (cyan) and S2 (magenta). (d, f) Resulting time course of mean ln LF (d) and ln HF (f) for the windowed segment. The red dashed line marks the transition onset (t = 0 s), colored segments show the linear regressions fitted over S1 and S2, and grey areas indicate periods outside these phases.

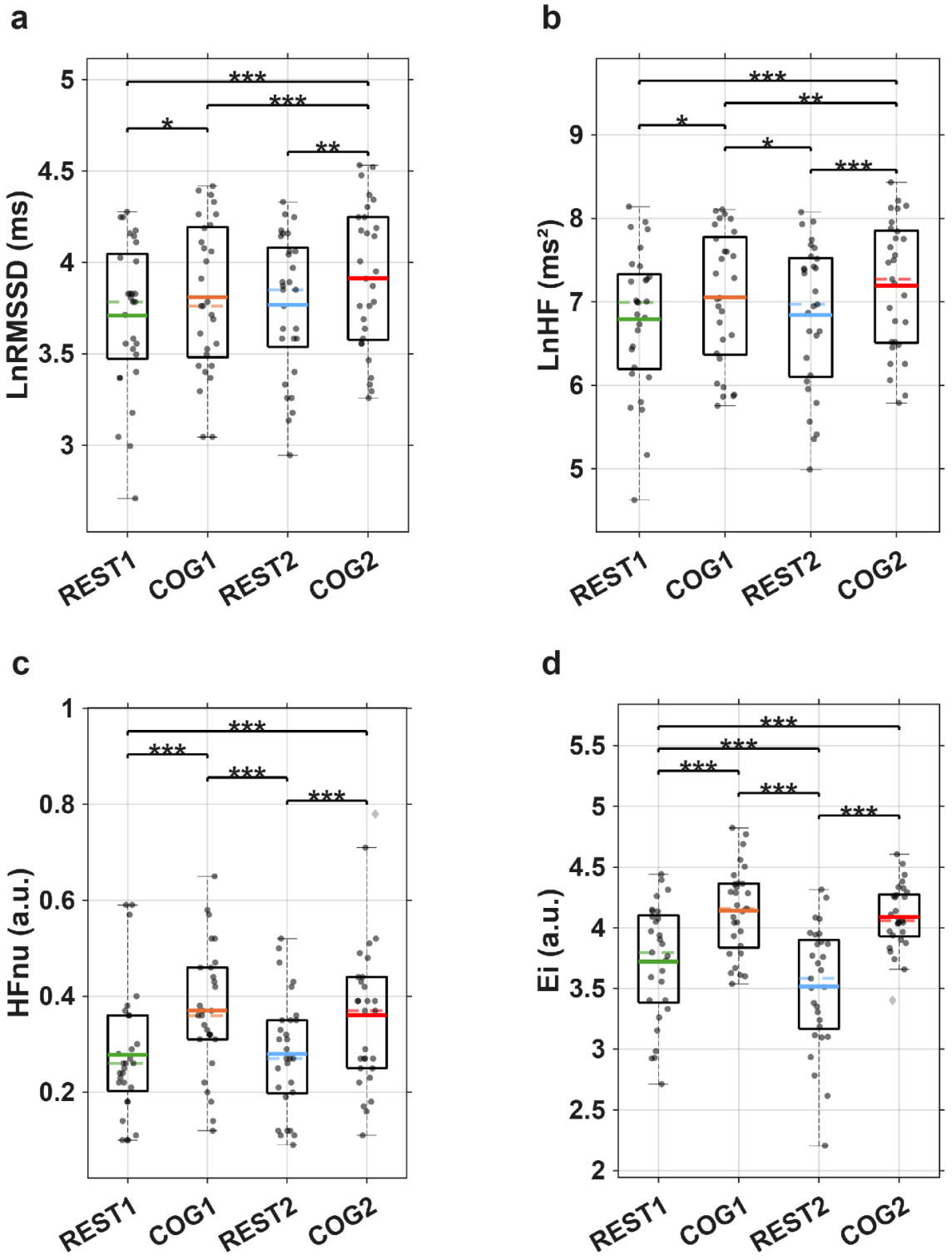

Figure 3

Box-and-whisker plots of heart rate variability and complexity markers across conditions (REST1, COG1, REST2, COG2). (a) Log-transformed root mean square of successive differences (LnRMSSD, ms). (b) Log-transformed high-frequency power (LnHF, ms²). (c) Normalized high-frequency power (HFnu, a.u.). (d) Entropy index (Ei, a.u.) computed with refined composite multiscale entropy (RCMSE). Solid lines

indicate means, dashed lines medians, boxes interquartile ranges (IQR), whiskers 1.5 × IQR, and black dots individual participants. *** p < 0.001, ** p < 0.01, * p < 0.05.

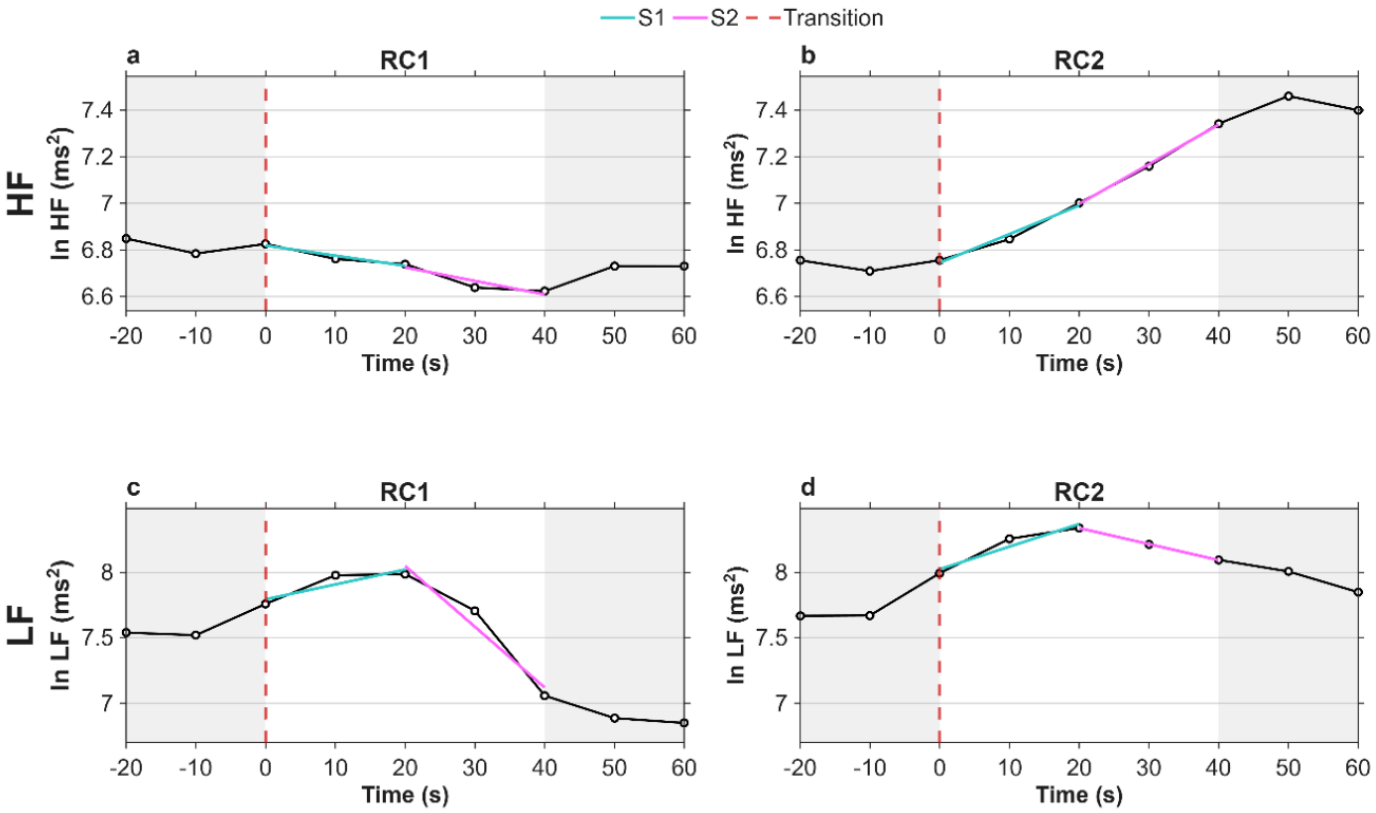

Figure 4

Time course of LnHF (top row, panels a–b) and LnLF (bottom row, panels c–d) during the two rest-to-task transitions, RC1 and RC2. The black line with open circles represents the mean time series. The red dashed vertical line marks the transition (t = 0 s). Colored segments show the linear regressions computed during the very-short-term (S1, cyan) and short-term (S2, magenta) responses. Periods outside these two phases are shaded in grey.

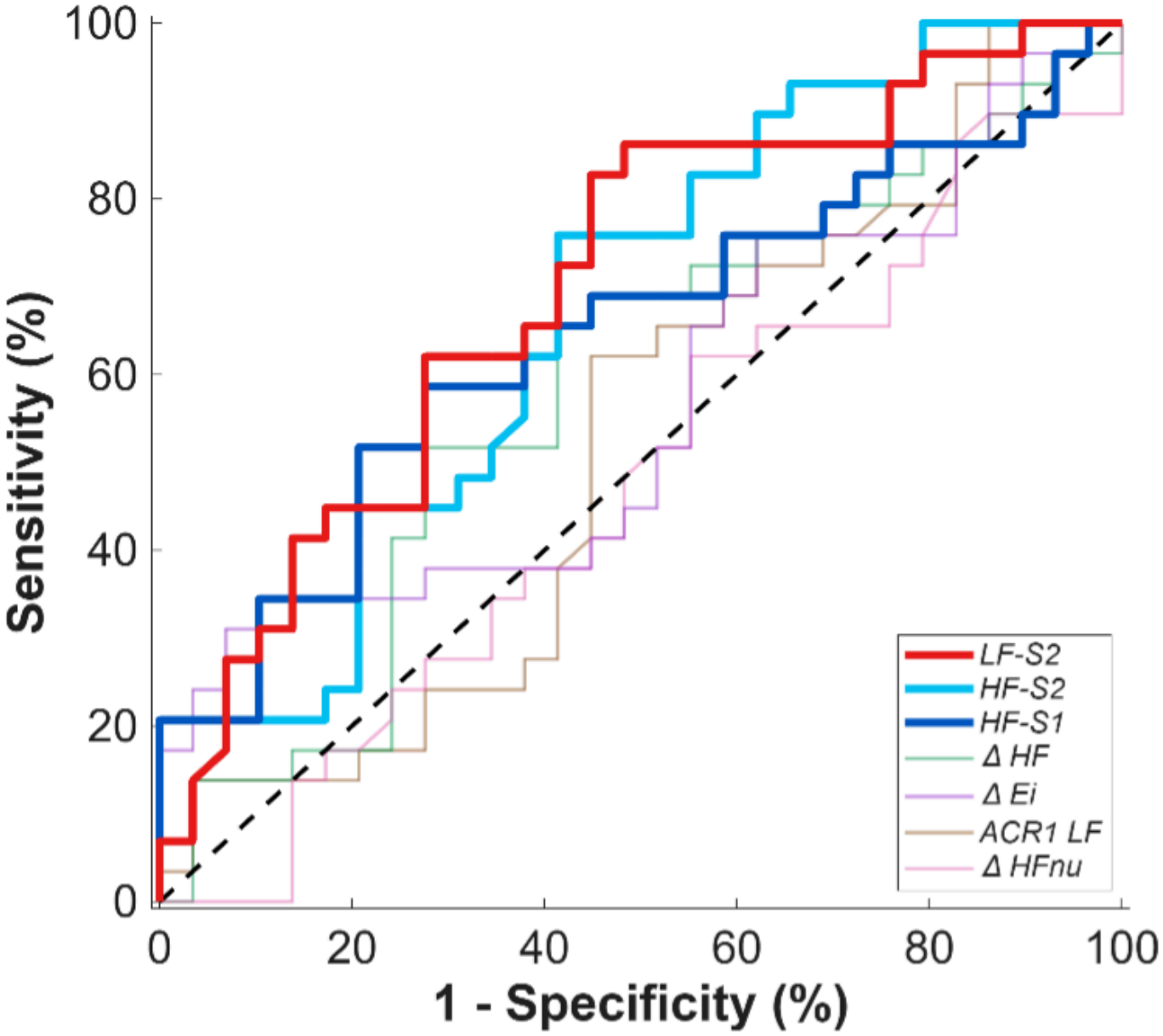

Figure 5

Receiver operating characteristic (ROC) curves of steady-state and transient HRV markers for discriminating RC2 (positive class) from RC1 (negative class). The dashed diagonal line represents chance-level discrimination (AUC = 0.5). The table summarizes the area under the ROC curve (AUC) and the corresponding J (Youden's index) for each marker.